Resonant x-ray Raman scattering from atoms and molecules

P.L. Cowan

Physics Division, Argonne National Laboratory, Argonne IL 60439

Abstract

Inelastic x-ray scattering and elastic x-ray scattering are fundamentally related processes. When the x-ray photon energy is near the ionization threshold for an inner shell, the inelastic channel is dominated by resonant x-ray Raman scattering. Studies of this emission not only illuminate the resonant scattering process in general, they also point to new opportunities for spectral studies of electronic structure using x-rays. Atoms in the form of a free gas provide an ideal target for testing the current theoretical understanding of resonant x-ray Raman scattering. In addition, x-ray scattering from molecular gases demonstrates the effect of bonding symmetry on the polarization and angular distribution of the scattered x-rays. Comparisons of experimental data with theory demonstrate both the successes and limitations of simple, single-electron interpretations of the scattering process.

1. Introduction

The central focus of this conference proceedings is anomalous scattering, which is an elastic x-ray scattering process. It has been discussed in other papers in these proceedings [1], and will be emphasized in this paper as well, that the elastic and inelastic x-ray scattering channels are intimately related. This fact has been demonstrated to be a direct consequence of the causality condition [2].

X-ray spectroscopy can be thought of as simply a manifestation of inelastic x-ray scattering [3]. Traditional x-ray spectroscopy, in turn has been categorized as either x-ray absorption spectroscopy (XAS) or x-ray emission spectroscopy (XES) [4]. Figure 1 schematically compares these two techniques. Simply put, XAS (fig.1a) is a probe of the unoccupied electronic states (above the Fermi energy, ε_F) of matter, while XES (fig.1b) probes the occupied levels (below the Fermi energy).

Figure 1. Schematic energy-level diagrams contrasting three types of spectroscopy. a) XAS - x-ray absorption spectroscopy; b) XES - x-ray emission spectroscopy; c) RXRS - resonant x-ray Raman scattering.

There are a number of characteristics of traditional x-ray spectroscopy which can be thought of as either advantages or disadvantages for studies of matter [5]. These characteristics, on the one hand, offer promise of experimental studies of the electronic and atomic structure of matter under a variety of conditions, but on the other hand, present obstacles such as lifetime broadening and satellite contamination.

This paper will focus on a particular case of x-ray inelastic-scattering spectroscopy, namely resonant x-ray Raman scattering (RXRS). Attention will be given to how this process relates to the canonical x-ray spectroscopy, to how RXRS relates to x-ray elastic scattering, and to how the peculiar characteristics of RXRS may be useful in overcoming the limitations of the other x-ray spectroscopic techniques.

Figure 1c shows a energy-level diagram representing "resonant x-ray Raman scattering". Unlike XAS and XES, x-ray Raman scattering is a two-photon process. The three diagrams of Figure 1 are suggestive of the relationship between each of the first two processes to the third. In the case of RXRS the net transition (broken arrow) is the promotion of an electron from one relatively high-lying occupied level to an unoccupied level. The deep inner-shell hole exists only in the virtual intermediate state.

Data illustrating resonant x-ray Raman scattering from argon are shown in figure 2 [6]. These emission spectra are observed near the energy of argon K-beta fluorescence, and are due to the net transition of

an Ar 3p electron to the 3p4p state*. Note that the energy difference between the RXRS peak and the elastic-scattered x-ray peak is constant as the incident energy is changed. This constant energy loss is reminiscent of the Stokes peak in optical Raman scattering [7], and is the reason for the choice of term "x-ray Raman scattering". Also note that since this energy loss depends only upon the energy interval of the net transition (fig 1c) the spectral width of the Raman peak will not be dependant upon the hole lifetime of the inner-shell. In other words, the RXRS need not suffer from the lifetime broadening observed in XAS (fig 1a) and XES (fig.1b)

There have been a number of papers on x-ray Raman scattering, and the particular case of resonant x-ray Raman scattering, most notably the pioneering experimental studies of Sparks [8], but most of this work has involved the more complicated case of scattering from solid samples. In studying the RXRS process it is desirable to begin with the case of scattering from a monatomic gas where the electronic structure is simplest. Results for RXRS from small molecules will also be presented to illustrate a number of additional RXRS effects.

Figure 2. Resonant x-ray Raman scattering from argon.

Figure 3. Schematic drawing of the experimental apparatus used for RXRS observations.

* The notation xxxyyy has been adopted for electronic configurations, where "xxx" indicates the hole states in otherwise filled levels and "yyy" indicates the occupancy of otherwise empty levels.

2. Experimental Method

The experimental techniques that have enabled studies of resonant x-ray Raman scattering from gases originated in studies of selective excitation of x-ray emission spectra [5]. This doubly differential x-ray spectroscopy was first demonstrated using laboratory x-ray techniques [10,11], but first become generally applicable with the advent of synchrotron radiation sources and tunable monochromators [12,13]. As will be discussed, observations have become increasingly differential, involving polarization analysis [14] and scattering-angle dependence [15] as well as spectroscopy vs. excitation and emission energies.

The measurements of resonant x-ray Raman scattering presented here were performed at the NIST-ANL x-ray beamline, denoted as X-24A [16], at the National Synchrotron Light Source (NSLS) at Brookhaven National Laboratory. A schematic of the instrumentation is shown in figure 3. X-rays from a bending magnet in the NSLS x-ray ring are filtered in energy, and their linear polarization is enhanced, by a tunable two-crystal monochromator [17]. The target, a gas confined in a cell for all cases under discussion, is then observed by a curved single-crystal spectrometer [18]. The secondary- spectrometer crystal disperses the emitted x-rays onto a position-sensitive detector [19]. With the sample placed well inside the Rowland circle of the instrument, the position-sensitive detector simultaneously collects photons within a given spectral region.

In some measurements the secondary spectrometer can also perform polarization analysis and/or determine the observation-angle dependence (with respect to incident polarization) of the spectra. The polarization selectivity of the secondary spectrometer stems from the fact that the x-ray equivalent of an optical Brewster's angle is very close to 45° [20]. Even when the incident angle is several degrees off of 45° sufficient polarization selectivity is obtained to observe the profound polarization effects that occur on sub-threshold resonances [14]. This leeway in Bragg angle permits measurements over a range of emission energies. It is also possible, within some limits, to improve the polarization selectivity at a given energy by one's choice of crystal. For example, Si(111) crystals have a Bragg angle of 44.5° at 2822 eV (roughly the energy of Chlorine Kβ fluorescence) while InSb(111) has a Bragg angle of 42.10° at 2472 eV (Sulfur Kβ).

3. Theoretical Background

X-ray emission excited near-threshold or on-resonance can best be described as an x-ray scattering process [3]. A theoretical basis for understanding this process can be found in the Kramers-Heisenberg

equation, which is derived by treating the electromagnetic-radiation field as a time-dependent perturbation acting upon a set of energy eigenstates of the atom or molecule under study [21].

Under the dipole approximation (i.e. $\exp(-i\mathbf{k}\cdot\mathbf{r}) \sim 1$) the differential cross section for a transition from state A to state B can be written as follows:

$$\frac{d\sigma_{AB}}{d\Omega} = r_e^2 \frac{\omega_2}{\omega_1} \left| \langle B|A\rangle \varepsilon_1 \cdot \varepsilon_2 + \frac{1}{m_e} \sum_I \frac{\langle B|p\cdot\varepsilon_2|I\rangle\langle I|p\cdot\varepsilon_1|A\rangle}{E_I - E_A - \hbar\omega_1 - i\Gamma_I/2} + \frac{1}{m_e} \sum_I \frac{\langle B|p\cdot\varepsilon_1|I\rangle\langle I|p\cdot\varepsilon_2|A\rangle}{E_I - E_A + \hbar\omega_2} \right|^2 \quad (1)$$

where the summation over I represents all possible intermediate states, ε_1 and ε_2 are the polarization vectors of the incident and final state photons, and all other symbols have traditional meanings. This is the so-called modified Kramers-Heisenberg equation which includes the $i\Gamma/2$ term in the denominator of the second term to account for intermediate-state lifetime. It is convenient, both heuristically and computationally to write the integration over continuum states as if it were a sum over discrete states. This is equivalent to assuming the atom is confined in a box. At any time one can take the limit as the energy spacing of the continuum states goes to zero (i.e. the sides of the box go to infinity). Also, it should be kept in mind that the sum over intermediate states will in general involve integration over hole-state-alignment and photoelectron-momentum directions as well as energy.

Figure 4. Feynman diagrams corresponding to each of the three terms in the Kramers-Heisenberg formula (eq. 1).

The three terms in the absolute value brackets can be identified with the three Feynman diagrams [21] shown in figure 4. The first term, sometime called the "Waller term" [22], is associated with the "sea gull" diagram (fig. 4a), and arises from to the $\mathbf{A}\cdot\mathbf{A}$ term in the interaction Hamiltonian. The other two terms come from the $\mathbf{p}\cdot\mathbf{A}$ interaction. By inspection of the denominators of these two terms, it is apparent that the middle term becomes large at or near resonance (i.e. $\hbar\omega_1 \cong E_I - E_A$), and it is referred to as the "resonant term".

As the associated diagram (fig. 4b) suggests, the resonant term resembles the probability of x-ray absorption (transition from state A to state I) followed by x-ray emission (state I to state B), and it is sometimes convenient to speak of the process in this way. However, the reader should keep in mind that, in cases where the primary x-rays are sufficiently monochromatic, the characteristic time for a photon-absorption event (i.e. the coherence time of the incident radiation) can be longer than the lifetime of the intermediate excited state (t_2-t_1). In this case, the concept of an x-ray absorption event followed independently by x-ray emission event is not entirely appropriate. It is important to note that the mathematical formalism of the Kramers-Heisenberg equation remains valid - only the Feynman diagrams become potentially misleading.

In order to compare the Kramers-Heisenberg theory to experiment, it is helpful to make a series of simplifying assumptions. A summary of those listed by Åberg et al [9,23] follows:

(1) The dipole approximation is used (as mentioned above).

(2) Only the resonant term is included except for elastic scattering (section 6).* If an orthogonal basis set of states are used for the states $|A\rangle$ and $|B\rangle$, the Waller term will become a Kronecker delta function in the dipole approximation

(3) The single electron approximation is used. (The inevitable breakdown of this assumption will be discussed below)

(4) The emitted electron is not detected (for cases with $\xi>0$)

Within these assumptions, Tulkki [23] has calculated the expected resonant x-ray Raman scattering cross section from argon using the modified Kramers-Heisenberg formula and Dirac-Folk wavefunctions. However, if a few additional assumptions and approximations are added, it is possible to construct an empirical model of the RXRS differential cross section, based on experimental measurements [6].

From assumption (4) the final state, $|B\rangle$ is indeterminant. Therefore, for comparison with RXRS experiments, one must also coherently sum (or integrate) eq. 1 over all final states, $|B\rangle$, consistent with the conservation of energy criterion

$$E_A + \hbar\omega_1 = E_I = E_B + \hbar\omega_2.$$

---

* Note that this assumption is in contrast to the "impulse approximation" [24] where only the first term (i.e. the $\mathbf{A}\cdot\mathbf{A}$ term) is included and multipole terms beyond the dipole are included. The impulse approximation is appropriate to high-energy Compton scattering.

In comparison to the ground-state energy, $E_A = 0$, the single-electron approximation is used to separate the excited-state energies, E_I and E_B, into electron energy plus hole-state energies, i.e.

$$\hbar\omega_1 = E_I + \xi_I = E_B + \xi_B + \hbar\omega_2$$

where the electron kinetic energy, $\xi<0$ for bound states*

Next one more assumption can be added:

(5) The electron excited by the initial photon acts as a spectator during the decay of the virtual hole state. This assumption has several consequences. First, it implies $\xi_I=\xi_B=\xi$. Second, the matrix element $\langle B|\mathbf{p}\cdot\varepsilon_2|I\rangle$ will be independent of the electron energy, ξ. Furthermore, the lifetime of the intermediate excited state, Γ_I, is also independent of the excited-electron energy (i.e. both radiative and non-radiative decay is insensitive to the spectator electron). Taken altogether this implies that the fluorescent yield is independent of the spectator-electron energy [25].

From the conservation of energy condition one can express the denominator of the resonant term as

$$E_I - E_A - \hbar\omega_1 - i\Gamma_I/2 = E_I - E_B - \hbar\omega_2 - i\Gamma_I/2$$

For inelastic photon scattering $\hbar\omega_1 \neq \hbar\omega_2$, the only remaining element of the resonant term which depends upon the electron excited state is the right matrix element which can be rewritten as

$$\langle I|\mathbf{p}\cdot\varepsilon_1|A\rangle = \langle I,\xi|\mathbf{p}\cdot\varepsilon_1|0,0\rangle = \langle I,\hbar\omega_1-E_B-\hbar\omega_2|\mathbf{p}\cdot\varepsilon_1|0,0\rangle$$

where the hole-state and electron energies are indicated separately. At this point one should note that the total photoelectric absorption cross section at $\hbar\omega_1$ is given by

$$\mu(\hbar\omega_1) \propto \left| \int \frac{\langle I,\xi|\mathbf{p}\cdot\varepsilon_1|0\rangle}{E_I+\xi-\hbar\omega_1-i\Gamma_1/2}\, d\xi \right|^2$$

which involves the convolution of the same matrix element with the Lorentzian lifetime broadening function. Finally, under the above

---

* It should be remembered that the Kramers-Heisenberg formula is derived under the assumption that coupling to the radiation field is a time-dependent perturbation to the energy eigenstates, and therefore the hole-state energies are well defined. Lifetime effects due to both radiative and non-radiative decay of the inner-shell hole, I, are accounted for by the $i\Gamma_I/2$ term in the denominator of the resonant term [21]

assumptions one can reduce the modified Kramers-Kronig equation for resonant inelastic x-ray scattering to

$$\frac{d^2\sigma(\hbar\omega_1)}{d\omega_2 d\Omega} \propto Y_{\underline{IB}} \left[(E_{\underline{I}} - E_{\underline{B}} - \hbar\omega_2)^2 - \Gamma_{\underline{I}}^2/4\right]^{-1} \mu^*(\hbar\omega_1 - \hbar\omega_2 + E_{\underline{I}} - E_{\underline{B}}) \qquad (2)$$

where μ^* represents the unconvolved photoelectric absorption function.

It may be instructive to make a close inspection of this result. First note that for constant final photon energy, $\hbar\omega_2$, the scattering function vs. $\hbar\omega_1$ should resemble a sharpened x-ray photoabsorption spectrum, much as has recently been reported [26]. The case where $\hbar\omega_1$ is fixed and the scattering spectrum vs. $\hbar\omega_2$ is observed is somewhat more complex. The negative sign on $\hbar\omega_2$ in the argument of μ^* suggests that the spectrum will again resemble an unconvolved XAS spectrum, but with the energy dependence inverted. However this mirror-image spectrum will be distorted by the $\hbar\omega_2$ dependence in the Lorentzian factor.

In addition to the relationship the x-ray absorption function, eq. 2 also indicates the evolution of RXRS to the familiar case of x-ray fluorescence emission. Simplistically, a typical x-ray absorption function resembles a step function with some near-edge structure, and the step occurring roughly at $\hbar\omega_1 = E_{\underline{I}}$. If $\hbar\omega_1 - E_{\underline{I}} >> \Gamma_{\underline{I}}$ the function μ^* should be roughly constant in the vicinity of $\hbar\omega_2 = E_{\underline{I}} - E_{\underline{B}}$ and the emission spectrum vs $\hbar\omega_2$ will be a uniformly filled Lorentzian function centered on the energy $E_{\underline{I}} - E_{\underline{B}}$, i.e. the expected x-ray fluorescence energy. When $\hbar\omega_1$ is below the edge μ^* will vanish in the vicinity of $\hbar\omega_2 = E_{\underline{I}} - E_{\underline{B}}$, where the lorentzian factor is large, and the RXRS will only be present for $\hbar\omega_2 < E_{\underline{I}} - E_{\underline{B}}$, i.e. in the low-energy wing of the Lorentzian factor. Thus, eq. 2 describes the Raman-like shift of the secondary-photon energy with as well as its decreased amplitude below the edge.

Later in the discussion, observations of polarization and anisotropic angular distribution of the resonant x-ray Raman scattering and elastic scattering will be presented. These effects are mathematically described in eq. 1 by the $\mathbf{p}\cdot\boldsymbol{\varepsilon}$ vectorial relations within the matrix elements in the resonant term, and in the case of elastic scattering, the $\boldsymbol{\varepsilon}_1\cdot\boldsymbol{\varepsilon}_2$ in the first term.

Since the resonant term involves a sum over intermediate states with all possible alignments, polarization or angular distribution from a particular transition will in general be masked by the superposition of transitions involving states of various symmetry. As will be shown, however, selective excitation permits observation of the x-ray

polarization and angular distribution from transitions with one, or predominantly one, type of symmetry.

4. RXRS from Atoms

To illustrate the successes and limitations of the theoretical model described above, it is convenient to begin with observations of resonant x-ray Raman scattering (RXRS) from monatomic gases. To date, such studies have been limited for technical reasons to observation of RXRS from argon near its K-shell threshold [6] and xenon near its L-shell thresholds [27]. In particular the case of RXRS from the ground state of Argon to the $\underline{2p}np$ (n=4,5...ξ) final states will be shown.

A recurring theme of RXRS studies has been the avoidance of lifetime broadening [5,25,28]. A variety of intuitive explanations have been offered, including analogies with "resonant fluorescence" [28,29], descriptions in terms of a virtual-coincidence measurement [5] and straight-forward energy-conservation arguments [23]. Evidence for this spectral narrowing* is shown in fig. 5 comparing Ar K-alpha emission spectrum excited well above threshold (but below excitation energies where satellite emission occurs [12]) to RXRS excited at the $\underline{1s}4p$ resonant excitation energy. While the change in FWHM is slight, this comparison is still indicative of the current state-of-the-art of such observations. The absence of Lorentzian tails, which are characteristic of lifetime broadening, (more evident on the log scale) is a clearer indication of the qualitative change that occurs in the shape of the peak for the RXRS case. It will become significant in latter discussion to note that the peak positions vs. emission energy are identical for excitation on-resonance and above-threshold.

Equation 2 offers a simple emperical method for calculating the RXRS spectra from the measured x-ray absorption spectrum. One must, however, generate such a spectrum unconvolved with the inner-shell lifetime. This might be accomplished via mathematical deconvolution or a measured x-ray absorption spectrum. Instead, figure 6 compares the measured argon K-edge absorption spectrum with a simple model [31]. The $\underline{1s}$-lifetime broadening can easily be removed from the mathematical model. The empirically determined parameters in this model include an energy and an oscillator strength for the prominent white-line resonance ($\underline{1s}4p$), a second oscillator strength for a Rydberg series (starting with $\underline{1s}5p$) leading featurelessly into the threshold and above [32], a Slater screening correction to the hydrogenic energy levels for the Rydberg series, a primary-monochromator Gaussian broadening,

---

* Line narrowing during RXRS was first reported by Eisenberg *etal* [30].

width and of course the 1s-hole lifetime. As seen in fig. 6, the agreement of the model with experiment is satisfactory with the lifetime-broadening value consistent with the accepted 0.69eV [33] and the monochromator adding an additional width of 0.4eV as expected for Si(111) crystals at 3.2keV [16] The other parameters are consistent with Watanabe's results [31].

Figure 5. Experimental evidence for decrease in lifetime broadening for resonant vs. non-resonant excitation of Ar Kα-like spectra. a) linear scale; b) log scale. Peaks have been artificially scaled to the same height.

Figure 6. Experimental argon K-edge absorption spectrum, and best-fit calculation from model. Arrows indicate the excitation energies of the RXRS spectra shown in fig. 7.

Figure 7. Linear and log plots of experimetal data for Kα-like argon RXRS. a) $\hbar\omega_1$= 3199.5eV, b) $\hbar\omega_1$= 3201.4eV,c) $\hbar\omega_1$=3203.3eV d) $\hbar\omega_1$=3204.3eV,e) $\hbar\omega_1$=3206.1eV, f) $\hbar\omega_1$=3219eV.

Figure 7 shows RXRS spectra for 2pnp final states observed for several primary x-ray energies. Spin-orbit splitting of the $2p_{1/2}$ and $2p_{3/2}$ inner-shell-hole states is easily resolved, and must be included in the model calculation. Due to the above-mentioned connection between RXRS and x-ray fluorescence above threshold, one can designate RXRS to

these states as K-alpha-like scattering.

Eq. 2 can be used to calculate the RXRS spectra using parameters from the emperical model for x-ray absorption. Several additional parameters specific to the scattering process must be determined. In principle the amplitude of the RXRS spectra could be calculated if the integrated flux, the secondary-spectrometer efficiency and the absolute fluorescent yields were known. However, efforts to integrate flux over the long accumulation times required for these data, have not been entirely satisfactory for this purpose [6], and the amplitude has been left as an adjustable parameter. The relative peak heights consistent with the expected statistical ratio of 2:1 and the spin-orbit splitting of the [2p]-hole levels to be consistent with accepted value [34] have been determined from the high-energy spectrum (fig. 7c). In the case of K-Alpha-like RXRS, the lifetime-broadening due to the [2p] levels must also be included [23]. This parameter, plus the Gaussian secondary-spectrometer resolution function are most sensitively tested using the sharp on-resonance RXRS data (fig. 7b), and again, the model matches well using the expected value of 0.26eV for the former, and the empirically determined value of 0.4eV for the latter [18].

Using the primary x-ray energy dependence given in eq. 2, the secondary spectra in fig.7 are compared to calculations with the over-all amplitude as the only remaining adjustable parameter. It is evident from these few example spectra that both the energy shift (especially note fig. 7a) and the qualitative shape of the spectra, including the peak narrowing, are well matched by the model. Small quantitative differences noticeable in the low-energy tails can be ascribed to the breakdown of specific assumptions [6].

Figure 8. Three-dimensional surface of RXRS differential cross section vs $\hbar\omega_1$ and $\hbar\omega_2$. Note the similarity of the two dimensional projections to XAS and XES spectra.

Given the apparent successes of the emperical model it is instructive to plot the predictions of the model vs. both $\hbar\omega_1$ and $\hbar\omega_2$. From fig 8, and from eq 2, it is evident that RXRS to a final state $|\underline{B},\xi>$

occurs along diagonals $\hbar\omega_1$-$\hbar\omega_2$=constant. The Lorentzian shape associated with the L-lifetime is evident along this diagonal, but not perpendicular to it. The projections of the 3D surface on the 2D surfaces (separately vs. $\hbar\omega_1$ and $\hbar\omega_2$) indicate how single-photon spectra inevitably exhibit the L-hole lifetime broadening. It is also apparent that whether the RXRS scattering is observed via a series of spectra versus $\hbar\omega_2$ at constant $\hbar\omega_1$ as presented in fig. 7 or as a spectrum vs. $\hbar\omega_1$ for constant $\hbar\omega_2$ [26] or a variety of other possible experimental strategies, the RXRS process offers the possibility of avoiding the resolution-limitation otherwise imposed upon x-ray spectra by short deep-inner-shell lifetimes.

However, it must be emphasized that the simple model represented above required an implicit series of simplifying assumptions. It is not surprising that examples of the failure of these assumptions are easily uncovered. Even for the case of atomic argon, the model that was relatively successful for Kα-like RXRS, fails rather dramatically for Kβ-like spectra [6]. The additional complications to RXRS due to the break-down of the above assumptions, plus those due to polarization and angular-distribution effects (which are explicitly included in the model) are most dramatically evident in observations of RXRS spectra from simple molecules.

5. RXRS from Molecules

5.1 Break-down of the spectator-electron assumption

Small molecules, specifically those containing chlorine, provide good testing ground for studying RXRS effects when the degeneracy and symmetry of atomic orbitals are lifted. RXRS involving the chlorine inner shells will be primarily sensitive to the molecular orbital wavefunctions in the vicinity of the Cl nucleus.

9. Resonant screening shift. a) Cl K-absorption spectrum for CF_3Cl b) satellite-free x-ray emission spectrum excited above threshold c) RXRS excited on-resonance.

Fig 9a shows the Cl K-edge XAS spectrum for CF_3Cl. The prominent white-line resonance is due to the promotion of the 1s electron to the unoccupied anti-bonding orbital [14]. Fig. 9b shows the above-threshold excited RXRS spectrum, which is typical of Cl Kβ fluorescence emission from this molecule, except that selective excitation has made it satellite-free [35]. One notes that, in contrast to Ar Kβ spectra (fig. 2), the splitting of the Cl-3p-like molecular-orbital levels is easily resolved.

Figure 9 contrasts the spectrum excited on-resonance to that excited above-threshold [36]. Unlike the case of Ar Kα-like spectra (fig. 5) the on-resonance peaks are shifted from their fluorescence positions. Furthermore, this shift is different for the various Cl-3p-like levels. This differential shift can be traced to screening differences between the 1s-hole intermediate state and the 3p-like-hole final state. In other words this indicates a failure of assumption (5), discussed above, that the excited electron acts as a spectator during the emission of the secondary x-ray. This assumption was a necessary criteria for establishing the simple relationship between RXRS spectra and XAS spectra. Thus, the derived relationship as indicated by eq. 2 is far from a general one. In cases where the 3p-like levels are not resolved, such as for Ar Kβ-like scattering, the differential-screening effect will tend to broaden the emission spectrum [6]. While this broadening is phenomenologically different from lifetime broadening, it will nevertheless tend to negate the narrowing due to the absence of hole-lifetime effects.

5.2 Polarization and Anisotropy of RXRS

As mentioned in Section 3, the vectorial nature of the momentum operator, $\mathbf{p}$, and the photon-polarization vectors, ε_1 & ε_2, in the Kramers-Heisenberg equation will describe in general the polarization dependence of RXRS. Since the photon's polarization is necessarily transverse to its wavevector, the angular distribution of RXRS may also become anisotropic. The mathematical predictions have been presented in detail elsewhere [37-40]. It may be helpful to gain some physical intuition into these effects by considering a schematic case (fig 10).

For simplicity, assume that an atom or molecule experiencing RXRS acts as a classical electric dipole oscillator*, first while absorbing a photon, then while re-emitting one. For a classical electric dipole oscillator, the angular distribution of the emitted radiation has a $\sin^2\theta$

---

* For an elegant example of x-ray polarization effects involving quadrupole transitions, see the work of Dräger et al [41]

dependence on polar angle, θ, with respect to the axis of the oscillation [42]. The emission is linearly polarized with the polarization vector in the plane defined by the emitted wave vector and the axis of the oscillator. Since absorption is equivalent to the time reversal of emission, similar relationships hold.

Figure 10. Schematic of polarization and anisotropy of RXRS due to virtual alignment of gas molecules.

Figure 11. Comparison of on-resonance XRS spectra observed for orthoginal polarizations.

Based upon these simplifying assumptions, it is possible to construct a schematic picture of how selectively excited x-ray emission, even from randomly oriented samples, can exhibit polarization and anisotropy. In fig. 10 the random alignment of molecules in a gas is represented by diagrams rotated by 90°. Pertinent molecular states and their relative symmetry are represented by closed circles and ellipses.

For the case depicted, methyl chloride, it is possible to select an excitation energy where the dominant allowed transition is the promotion of a Cl 1s-electron, indicated by the letter K, to an unoccupied anti-bonding state. The dipole selection rules will limit absorption (and emission) transitions to molecular orbitals with p-like wavefunctions. The classical oscillator corresponding to this transition has its axis along the C-Cl bond, so for linearly polarized primary radiation (represented by the double-headed arrow) those molecules oriented transverse to the polarization (as on the right of fig. 10) will have vanishing excitation probability. Those molecules which are instantaneously aligned with the E-field (as on the left) will have a significant absorption cross section, with a continuously varying amplitude for intermediate orientations. The result will be the creation of a partially aligned ensemble of core-hole excited molecules within the overall random collection of molecules.

The lower part of fig. 10 depicts the emission processes from this

aligned, excited ensemble of molecules. One possibility (case 1) is a transition of a Cl-3p-like bonding electron, B, to the hole in the K-shell. This transition also will act like an oscillator aligned along the bond axis, so the emission will tend to be directed perpendicular to this axis (as represented by the outgoing wavelets) and the linear polarization will be parallel to that of the primary x-rays. Alternatively (case 2), the K-hole may be filled by a non-bonding 3p-electron, N. The transitions from these levels will act like dipole oscillators oriented transverse to the bond axis, so both the direction and polarization of this emission will tend to be 90° away from that due to the bonding electrons. The molecules in the right hand column of fig. 10 show no emission because there has been no absorption.

The molecules can be considered to be stationary since the lifetime of the core hole is short (roughly, femtoseconds) compared to the time scale of molecular reorientation (picoseconds). However, the observed polarization and anisotropy must be averaged in three dimensions over all alignment angles. The net polarization and anisotropy resulting from a classical dipole model has been quantitatively described previously [37,38]. Rigorous quantum mechanical treatments of these phenomena have also been developed [39,40].

In order to observe polarization and anisotropy characteristic of a classical dipole radiator, the x-ray emission from transitions with a given symmetry must be resolvable from other emitting transitions. This is partially true for the case of methyl chloride [14], and is realized even more completely in other cases [43,44], for example CF_3Cl. Figure 11 compares the RXRS spectra for orthogonal secondary-photon polarization from CF_3Cl excited on-resonance [43]. The spectra have been artificially scaled to match the heights of largest peak, that associated with the non-bonding Cl-3p-like orbitals. The change in the relative heights of the other spectral peaks to the largest is unmistakable.

Figure 12. Observation-angle dependance of RXRS for three spectral features from CF_3Cl compared to theoretical expectations.

Figure 13. Resonant depolarization of elastic x-ray scattering from $CFCl_3$

Comparisons similar to fig. 11 of spectra observed at different observation angles have been reported [15]. Figure 12 plots the ratio of spectral peak heights versus the observation angle, β indicated in fig 3. For molecular samples these observations are conceptually equivalent to rotating the primary x-ray polarization [45].

Studies of polarization and anisotropy of RXRS have begun to be applied to problems such as the determination of molecular-orbital symmetry [46], and offer the potential for rough determination of atomic, as well as electronic, structure of molecules in randomly aligned systems.

5.3 Resonant Depolarization of Elastic X-ray Scattering

While elastic x-ray scattering from molecular gases falls outside the definition of resonant x-ray Raman scattering, studies of this phenomena are nevertheless of some relevance to this conference as a whole, and also serve to illuminate additional aspects of the Kramers-Heisenberg predictions. Studies of elastic scattering easily permit one to examine the case where both the Waller term and the resonant term contribute significantly to the scattering cross section. In particular, the polarization dependence for the two term differ, and the interference between these terms can be expected to change significantly in the vicinity of a resonance.

It is well known that elastically scattered x-rays are linearly polarized perpendicularly to the scattering plane (s-polarized) when the scattering angle is 90°. At 90° the dipole approximation used to derive eq. 1 breaks down for the first ($\mathbf{A}\cdot\mathbf{A}$) term. Finkelstein [47] has presented evidence of the importance of quadrupole terms in elastic scattering. However, the polarization dependence (but not the absolute amplitude) of the data presented here is adequately treated with the dipole approximation. On resonance the elastic scattered emission can become depolarized via contribution from the resonant term. Except for fact that different final states are reached, the resulting depolarization of elastic x-ray scattering results from the same resonant term that produces the polarization of RXRS.

The results of measurements [45,47] of the polarization of elasticly scattered x-rays observed at a 90° scattering angle for polarized incident x-rays are shown in figure 13. The polarization is plotted as a function of energy near the Cl K-edge of $CFCl_3$. On the same abscissa the x-ray absorption spectrum is shown for reference. Clearly the strong depolarization observed for the elastic scattered x-rays is correlated with the large sub-threshold absorption resonance at 2823eV.

Measurements of the angular dependence of elastic x-ray scattering from matter is a well established method of determining structure on the atomic scale. All of x-ray crystallography is based on this process.

Unlike crystals, however, molecules in a gas cannot be mounted on a goniometer and oriented with respect to the incident wavevector. However, studies of the resonance dependence of scattering can potentially provide information about partially aligned molecules. Put another way, the depolarization effect may act as a virtual goniometer for molecules.

6. Conclusion.

Resonant x-ray Raman scattering (RXRS) offers a genuine opportunity to employ x-rays for spectroscopic studies that are not affected by inner-shell- hole lifetimes. However, the simple one-electron picture of the RXRS process can easily breakdown. This is both a complication, in terms of direct application of the method, and an opportunity, for those interested in studies of many-electron phenomena. Beyond the new opportunities for strictly spectroscopic studies, measurements of polarization and angular distribution of RXRS offers the additional possibilities of determination of local electronic and atomic symmetry and structure in disordered systems.

7. Acknowledgments

The author wishes to acknowledge the following collaborators who have contributed over the years to the results presented here: J. Cooper, A. Henins, T. Jach, D.W. Lindle, R.C.C. Perera and S.H. Southworth. Special acknowledgements are due to R.D. Deslattes and R.E. LaVilla who got the author started in this direction, to S. Brennan and B.A. Karlin without whom nothing at all would have been accomplished at NSLS beamline X-24A and to T. Åberg and B. Crasemann for helpful discussions on the theory of RXRS. This work was supported by the U.S. Department of Energy Nuclear Physics Division, under contract W-31-109-ENG-38.

8. References

1. For example see L.B. Sorenson, J.O. Cross, J.J. Rehr, H. Stragier, C.E. Bouldin and J.C. Woicik, these proceedings.
2. H.A. Kramers, Atti Congr.Intern.Fis.Como 2 545 (1927); R. Kronig, J.Opt.Soc.Am. 12 547 (1926).
3. T. Åberg, Phys.Rev.156, 35 (1967); T. Åberg, Physica Scripta 21, 495 (1980).
4. L.G. Parratt, Rev.Mod.Phys. 31, 616 (1959).
5. P.L. Cowan, Physica Scripta T31, 112 (1990).
6. P.L. Cowan, S. Brennan, J. Cooper, R.D. Deslattes, T. Jach, B.A. Karlin and R.E. Lavilla, in preparation.
7. C.V. Raman, Ind.J.Phys. 2, 387 (1928); For a comprehensive review

see Raman Effect, ed. A. Anderson (Marcel Dekker, Inc., New York, 1971).
8. C.J. Sparks, Phys. Rev. Lett. 33 262 (1974); for a comprehensive list of references to previous work on x-ray Raman scattering see ref.
9.
9. T. Åberg and B. Crasemann, these proceedings.
10. R.D. Deslattes, Phys.Rev.133, A390 (1964); R.D. Deslattes, Phys.Rev. 133, A399 (1964);
11. R.C.C. Perera, J. Barth, R.E. LaVilla, R.D. Deslattes and A. Henins, Phys.Rev.A 32, 1489 (1985).
12. R.D. Deslattes, R.E. LaVilla, P.L. Cowan, A. Henins, Phys.Rev A 27, 923 (1983); R.D. Deslattes, P.L. Cowan, R.E. LaVilla and K. Dyall, AIP Conf. Proc. 94, 100 (182).
13. R.D. Deslattes, Aust. J Phys. 39, 845 (1986); R.D. Deslattes, J.de Phys. 48, C9-579 (1987).
14. D.W. Lindle, P.L. Cowan, R.E. LaVilla, T. Jach, R.D. Deslattes, B.A. Karlin, J.A. Sheehy, T.J. Gil and P.W. Langhoff, Phys.Rev.Lett. 60, 1010 (1988)
15. S.H. Southworth, D.W. Lindle, R. Mayer and P.L. Cowan, Phys. Rev. Lett. 67 1098 (1991); S.H. Southworth, D.W. Lindle, R. Mayer and P.L. Cowan, Nucl. Instrum. Meth. B 56/57 304 (1991).
16. P.L. Cowan, S. Brennan, R.D. Deslattes, A. Henins, T. Jach and E.G. Kessler, Nucl. Instrum and Meth. A 246, 154 (1986); P.L. Cowan, S. Brennan, T. Jach, D.W. Lindle, and B.A. Karlin, Rev. Sci. Instrum. 60 1603 (1989).
17. P.L. Cowan, J.B. Hastings, T. Jach and J. Kirkland, Nucl. Instrum. and Meth. 208, 349 (1983).
18. S. Brennan, P.L. Cowan, R.D. Deslattes, A. Henins, D.W. Lindle and B.A. Karlin, Rev. Sci. Instrum. 60 2243 (1989).
19. B. Duval, J. Barth, R.D. Deslattes, A. Henins and G. G. Luther, Nucl. Instrum. and Meth. 222, 274 (1984).
20. M. Hart and A.R.D. Rodrigues, Phil Mag. B 40, 149 (1979).
21. J.J. Sakurai, Modern Quantum Mechanics, (Benjamin/Cummings, 1985).
22. J. Bremer, J. Phys. B 12, 2797 (1979).
23. J. Tulkii and T. Åberg, J. Phys. B 15, L435 (1982); J. Tulkki, Phys. Rev. A 27, 3375 (1983).
24. P. Eisenberger and P.M. Platzman, Phys.Rev.A 2, 415 (1970).
25. Rencent measurements of the excitation-energy dependence of the argon K-fluorescent yield [T. LeBrun et al, in preparation] have determined that such efects are at the few-percent level
26. K. Hämäläinen, D. P. Siddons, J. B. Hastings and L. E. Berman, Phys. Rev. Lett. 67 2850 (1991).
27. R.D. Deslattes, P.L. Cowan, B.A. Karlin, T. LeBrun, J. Levin and

S.H. Southworth, in preparation.
28. G.S. Brown, M. H. Chen, B. Crasemann and G. E. Ice, Phys. Rev. Lett. **45**, 1937 (1980); G. E. Ice, G. S. Brown, G. B. Armen, M. H. Chen, B. Crasemann, J. Levin and D. Mitchell, AIP Conf. Proc. **94**, 105 (1982); G. B. Armen, T. Åberg, J. Levin, G. E. Ice, G. S. Brown and B. Crasemann, Phys. Rev. Lett. **54** 1142 (1985).
29. W. Heitler, The Quantum Theory of Radiation, (Clarendon Press, Oxford, 1954).
30. P. Eisenberger, P. M. Platzman and H. Winick, Phys. Rev. Lett. **36** 623 (1976). P. Eisenberger, P. M. Platzman and H. Winick, Phys. Rev. B **13**, 2377 (1976).
31. T. Watanabe, Phys. Rev. **139**, A1747 (1965).
32. U. Fano and J.W. Cooper, Rev.Mod.Phys. **40**, 441 (1968).
33. M.O. Krause and J.H. Oliver, J.Chem.Phys.Ref.Data **8**, 329 (1979).
34. P. Richard, M. Stockli, R.D. Deslattes, P. Cowan, R.E. LaVilla, B. Johnson, K. Jones, M. Meron, R. Mann and K. Schartner, Phys. Rev. A **29**, 2939 (1984).
35. R. C. C. Perera, P. L. Cowan, D. W. Lindle, R. E. LaVilla, T. Jach and R. D. Deslattes, Phys. Rev A **43**, 3609 (1991).
36. R.C.C. Perera, R.E. Lavilla, P.L. Cowan, T. Jach and B. Karlin, Phys. Scripta **36**, 132 (1987); R.C.C. Perera, P.L. Cowan, D.W. Lindle and R.E. Lavilla, J. de Phys. **48**, C9-753 (1987).
37. R. N. Zare, Angular Momentum, (John Wiley, New York, 1988).
38. U. Fano and J. H. Macek, Rev.Mod.Phys. **45**, 553 (1973).
39. F.Kh. Gelmukhanov and L.N. Mazalov, Pot.Spectrosc. **42**, 371 (1977).
40. C.H. Green and R.N. Zare, Ann.Rev.Phys.Chem. **33**, 119 (1982).
41. J. D. Jackson, Classical Electrodynamics, (John Wiley, New York, 1962).
42. G. Dräger, AIP Conf.Proc **215**, 700 (1991); G. Dräger and W. Czolbe, these proceedings.
43. D.W. Lindle, P.L. Cowan, R.E. LaVilla, T. Jach, R.C.C. Perera and R.D. Deslattes, J. de Phys. **48** C9-761 (1987).
44. D.W. Lindle, P.L. Cowan, R.E. LaVilla, T. Jach, R.D. Deslattes, R.C.C. Perera, B. Karlin, SPIE **911**, 54 (1988); D.W. Lindle, P.L. Cowan, R.E. LaVilla, R.D. Deslattes, Nucl.Instrum and Meth. B **40/41** 257 (1989); D.W. Lindle, P.L. Cowan, T. Jach, R.E. LaVilla, R.D. Deslattes, and R.C.C. Perera, Phys.Rev. A **43**, 2353 (1991).
45. P.L. Cowan, AIP Conf. Proc. **215**, 696 (1991) .
46. R. Mayer, D.W. Lindle, S.H. Southworth and P.L. Cowan, Phys.Rev.A **43**, 235 (1991).
47. K.D. Finkelstein and Q. Shen, these proceedings.
48. P.L. Cowan, D.W. Lindle, S. Southworth and B. Karlin, in preparation.

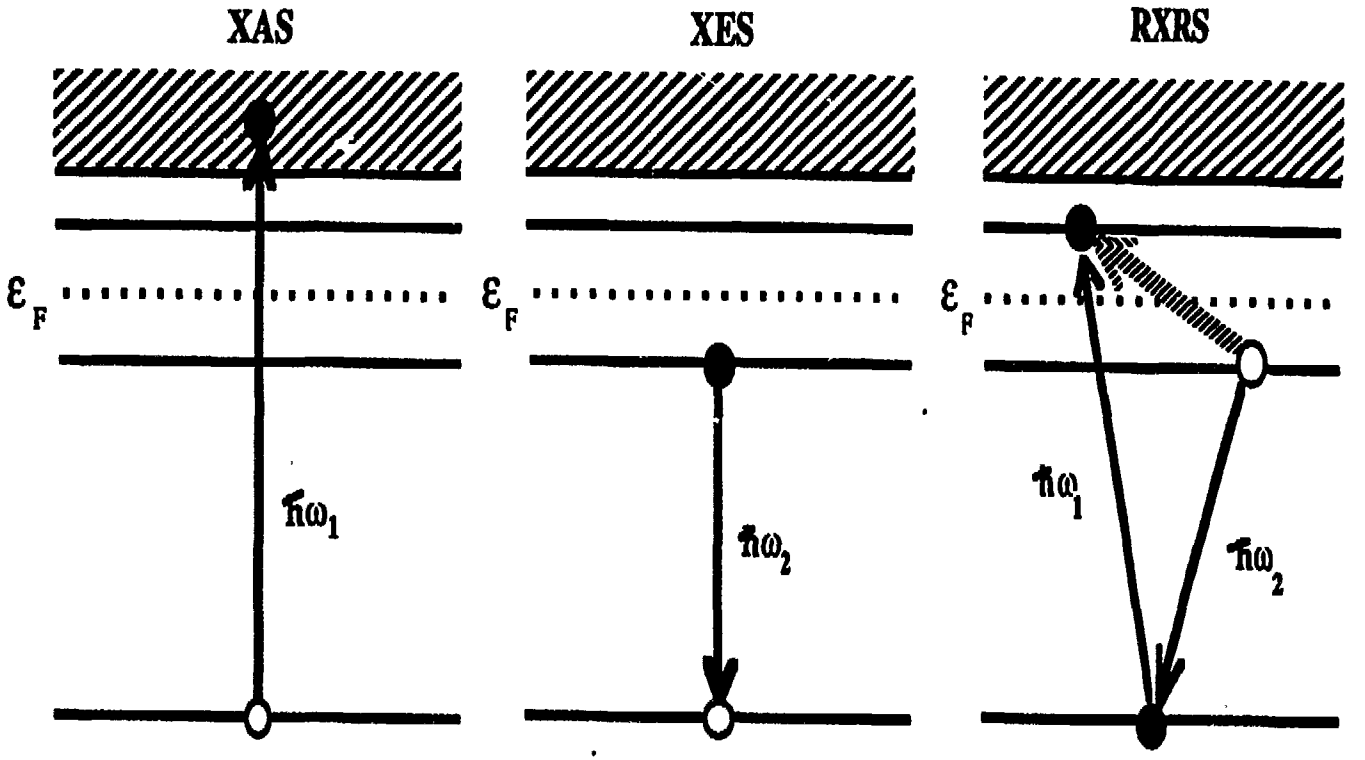
XAS
XES
RXRS
ε_F
ε_F
ε_F
$\hbar\omega_1$
$\hbar\omega_2$
$\hbar\omega_1$
$\hbar\omega_2$

fig 1

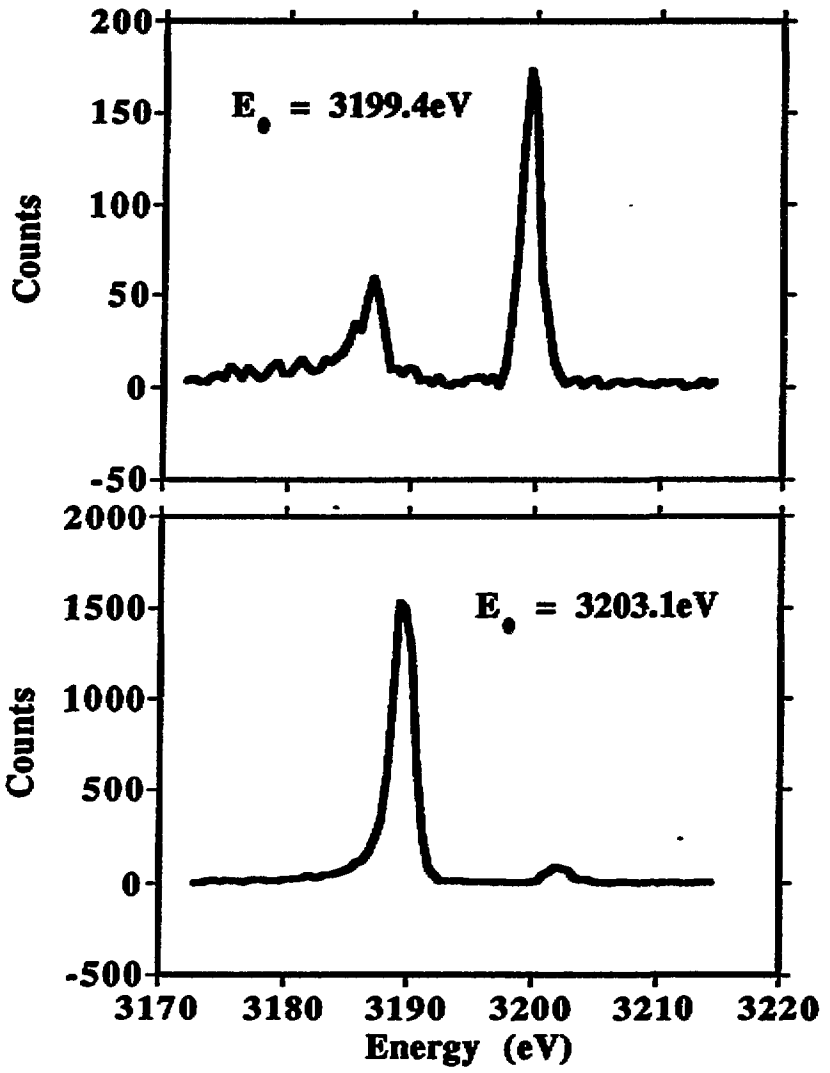
200
150
100
50
0
-50
Counts
E$_e$ = 3199.4eV
2000
1500
1000
500
0
-500
Counts
E$_e$ = 3203.1eV
3170
3180
3190
3200
3210
3220
Energy (eV)

fig 2

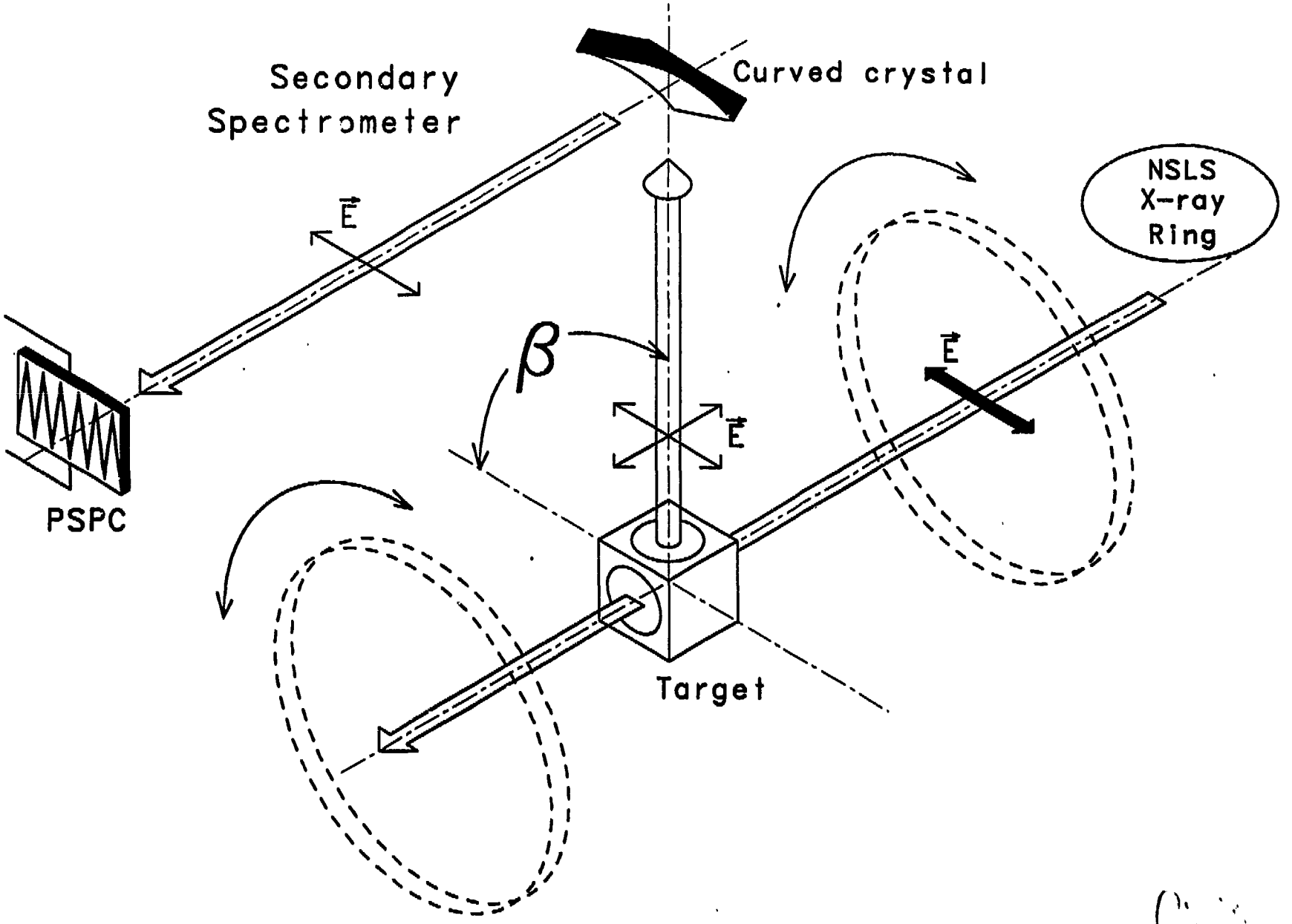
Secondary
Spectrometer
Curved crystal
NSLS
X-ray
Ring
$\vec{E}$
β
$\vec{E}$
$\vec{E}$
PSPC
Target

fig 3

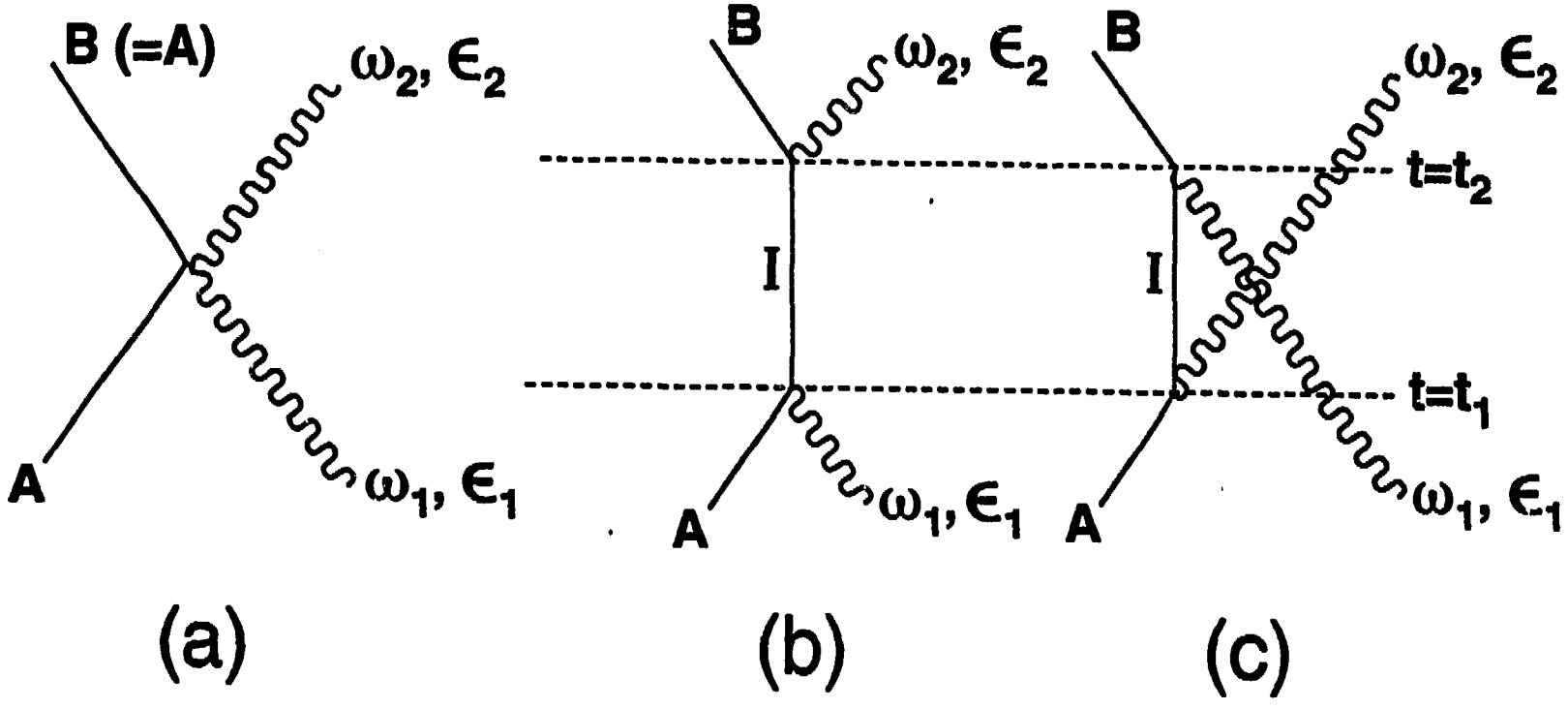
B (=A)
ω_2, ϵ_2
A
ω_1, ϵ_1
B
ω_2, ϵ_2
I
A
ω_1, ϵ_1
B
ω_2, ϵ_2
$t=t_2$
I
$t=t_1$
A
ω_1, ϵ_1
(a)
(b)
(c)

fig 4

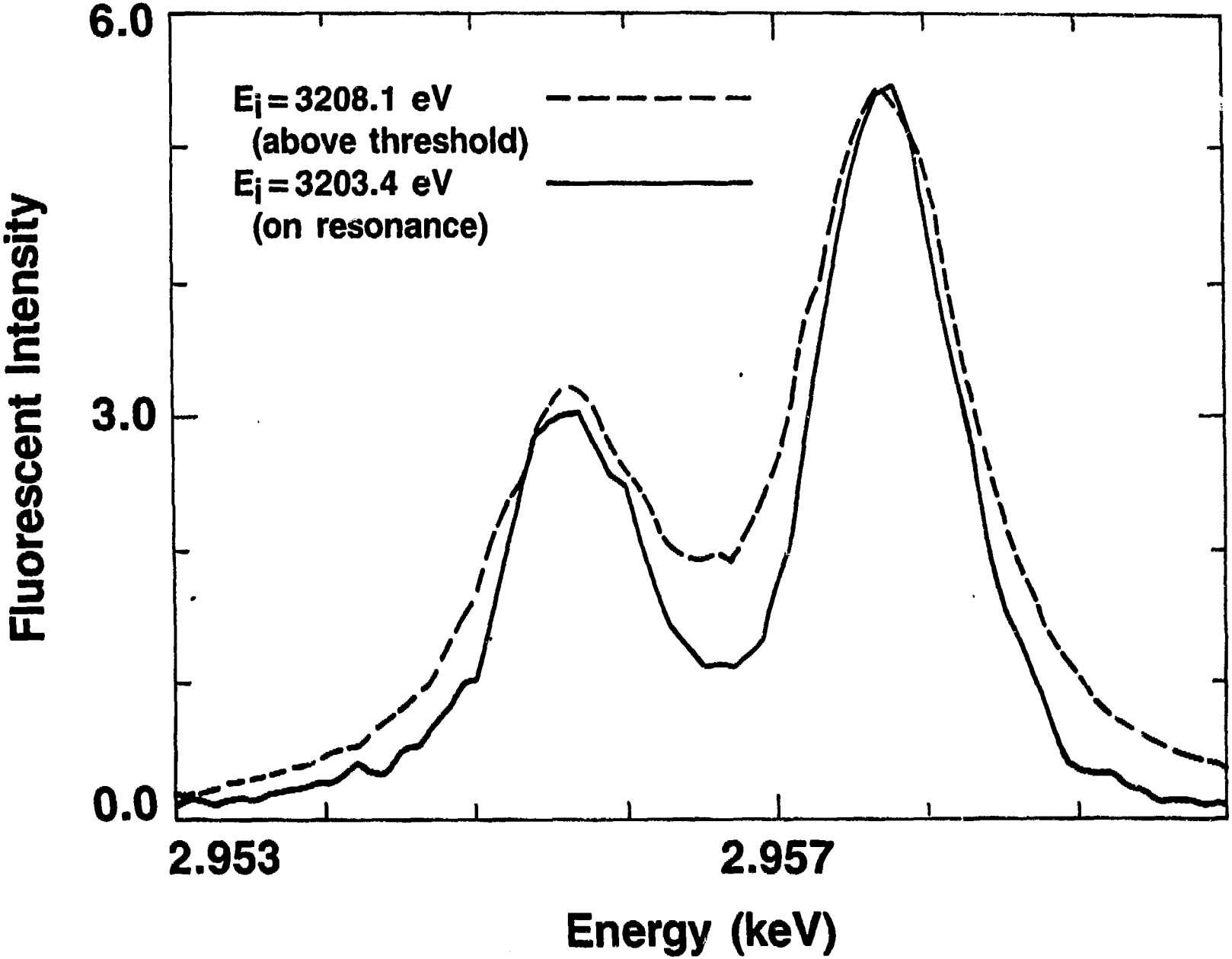
6.0
3.0
0.0
Fluorescent Intensity
$E_i = 3208.1$ eV
(above threshold)
$E_i = 3203.4$ eV
(on resonance)
2.953
2.957
Energy (keV)

fig 5

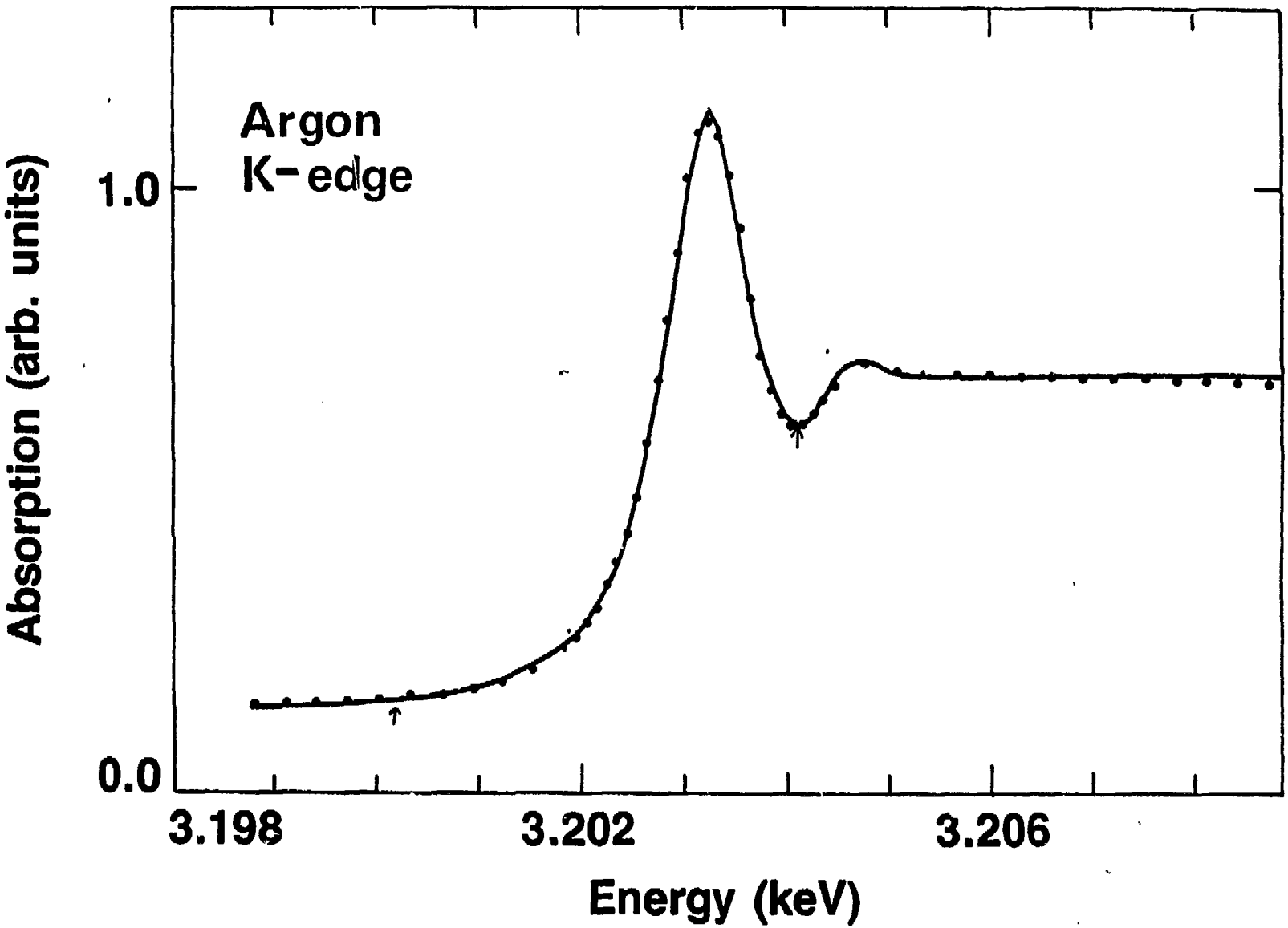
Argon
K-edge
1.0
0.0
Absorption (arb. units)
3.198
3.202
3.206
Energy (keV)

fig 6

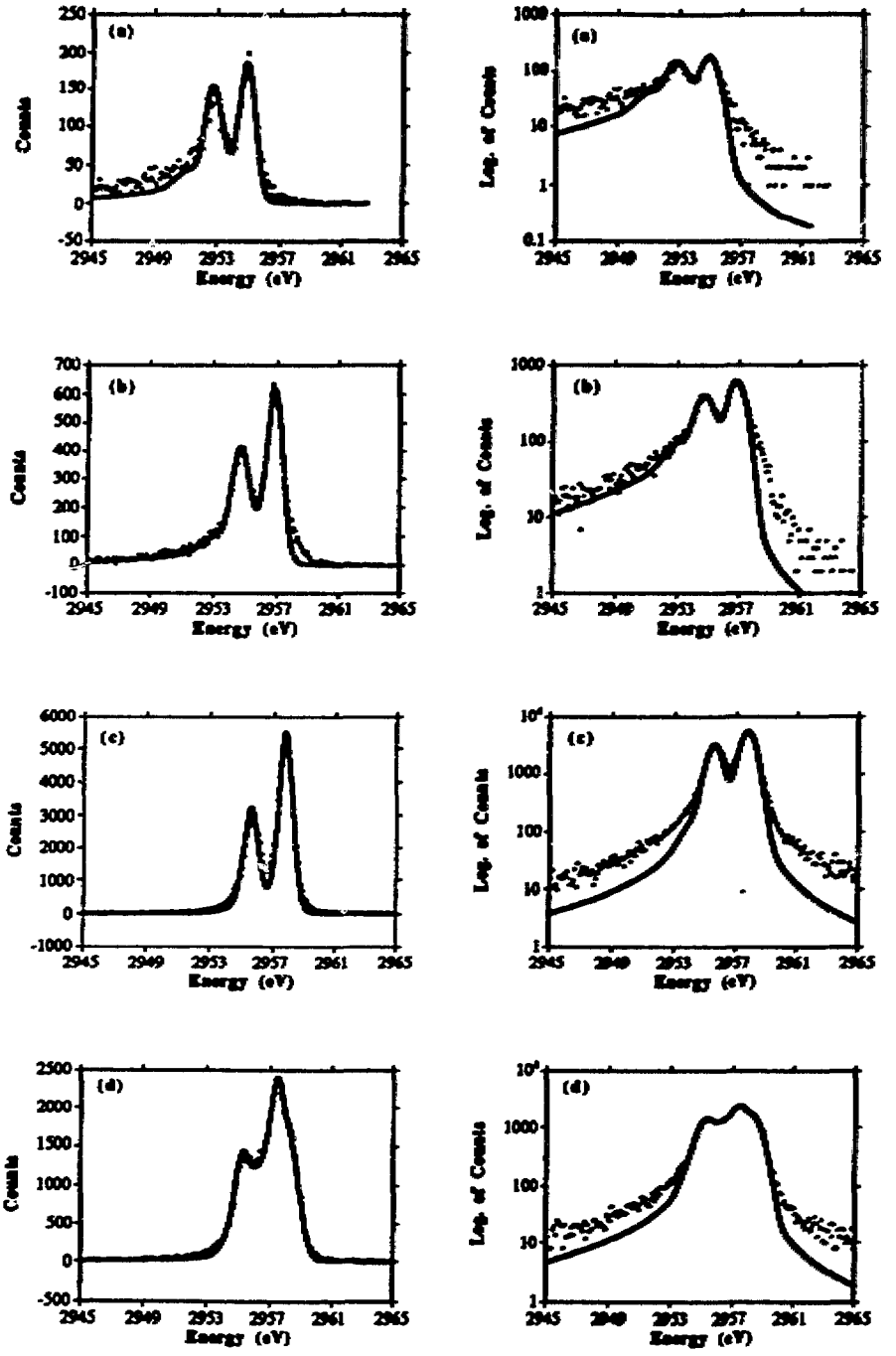

fig 7

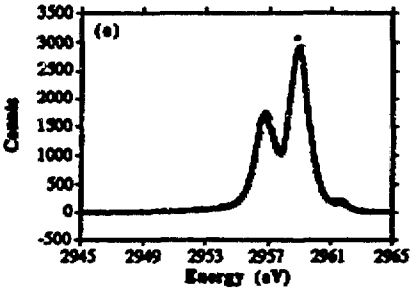
(e)
Counts
Energy (eV)

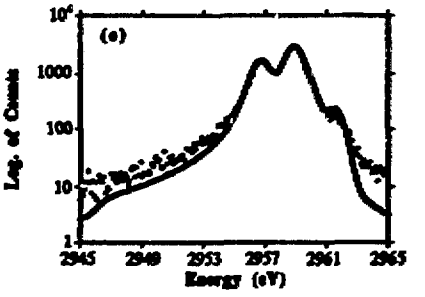
(e)
Log. of Counts
Energy (eV)

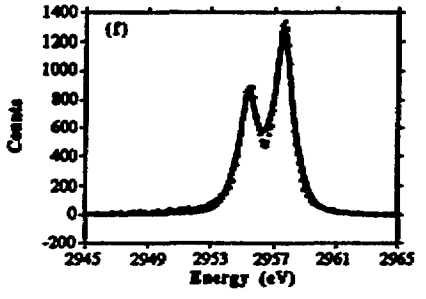
(f)
Counts
Energy (eV)

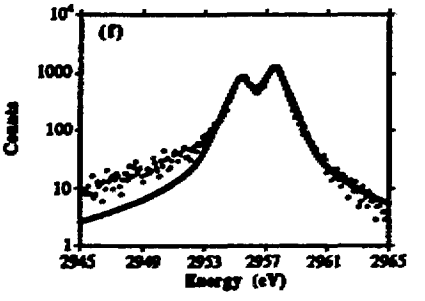
(f)
Counts
Energy (eV)

fig 7 (cont)

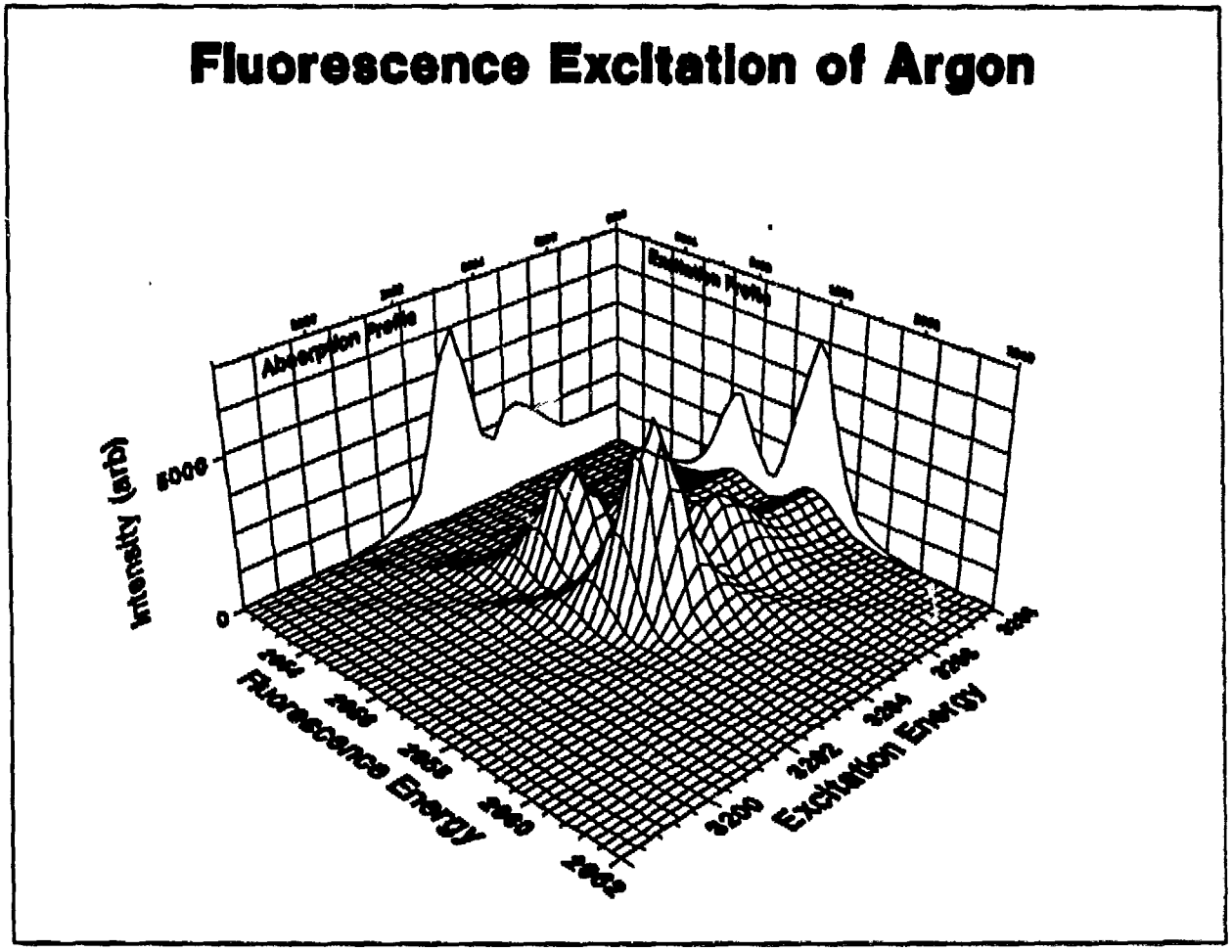
Fluorescence Excitation of Argon
Absorption Profile
Emission Profile
Intensity (arb)
8000
0
Fluorescence Energy
Excitation Energy

fig 8

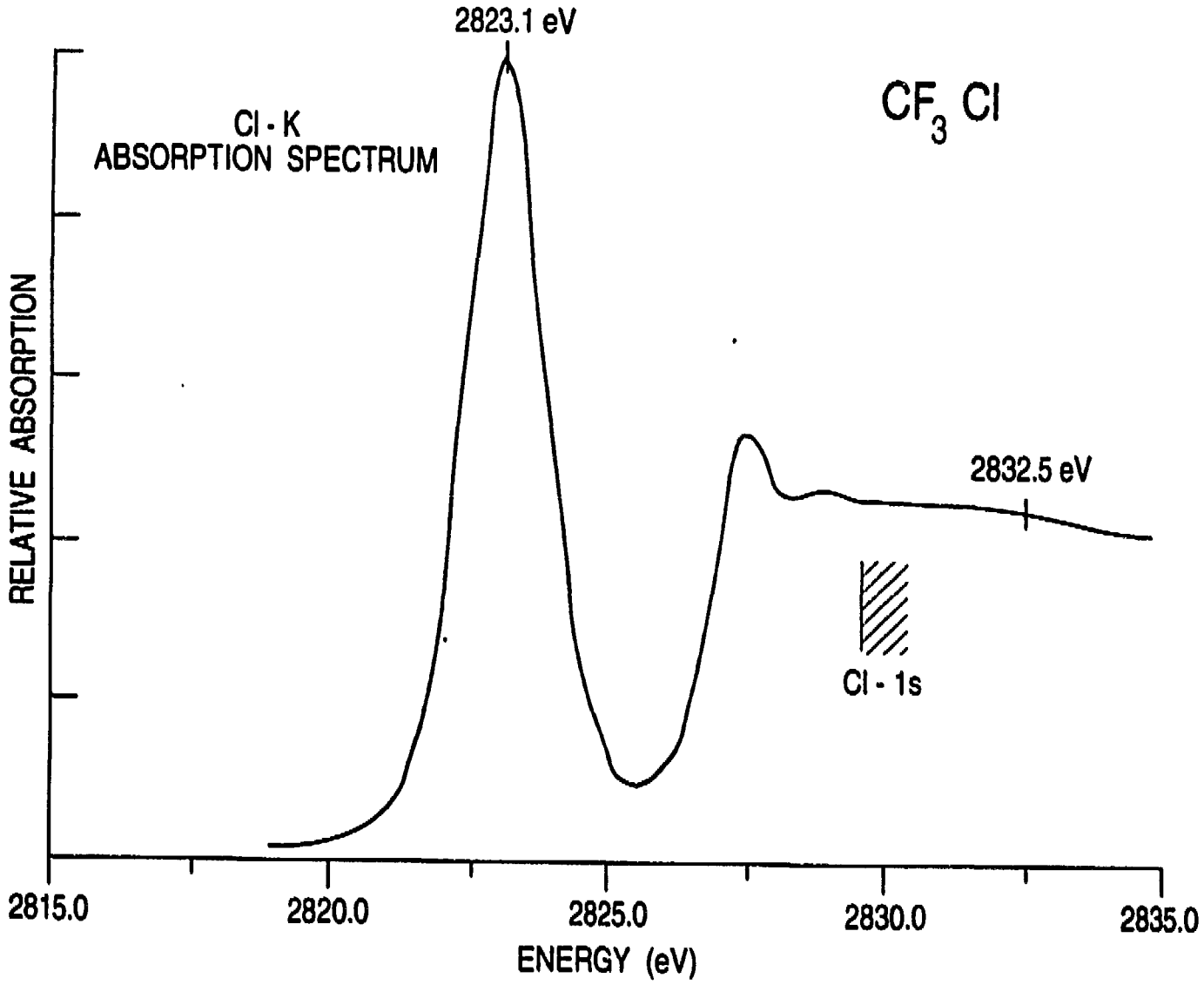
2823.1 eV
Cl - K
ABSORPTION SPECTRUM
CF_3 Cl
RELATIVE ABSORPTION
2832.5 eV
Cl - 1s
2815.0
2820.0
2825.0
2830.0
2835.0
ENERGY (eV)

Fig 9a

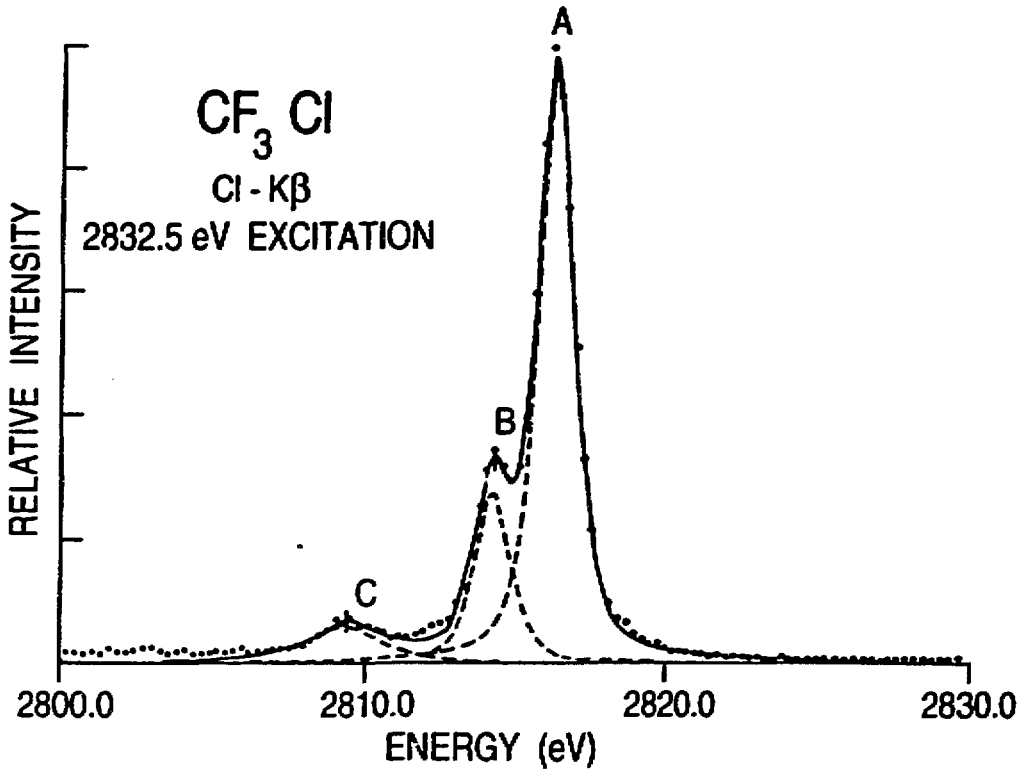
CF_3Cl
Cl - Kβ
2832.5 eV EXCITATION
RELATIVE INTENSITY
A
B
C
2800.0
2810.0
2820.0
2830.0
ENERGY (eV)

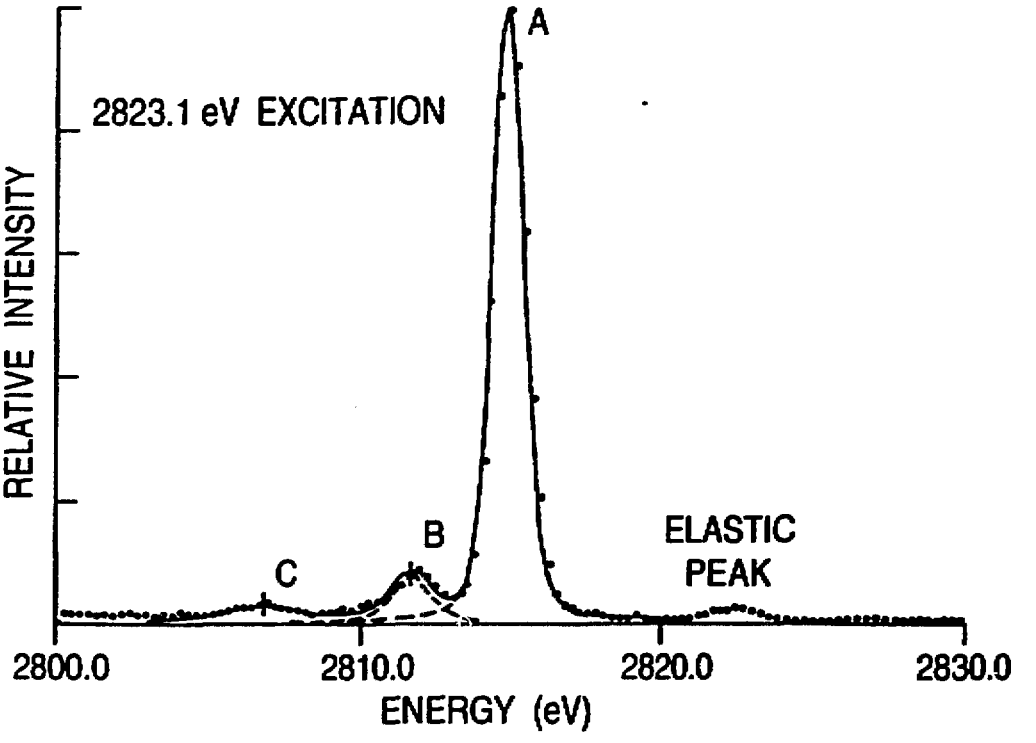
2823.1 eV EXCITATION
RELATIVE INTENSITY
A
B
C
ELASTIC
PEAK
2800.0
2810.0
2820.0
2830.0
ENERGY (eV)

Fig 9b,c

Absorption

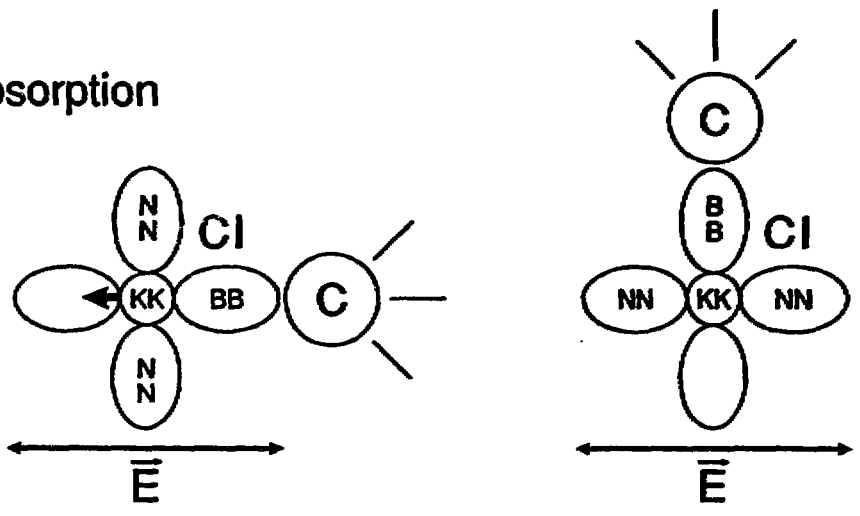

Emission: Case 1

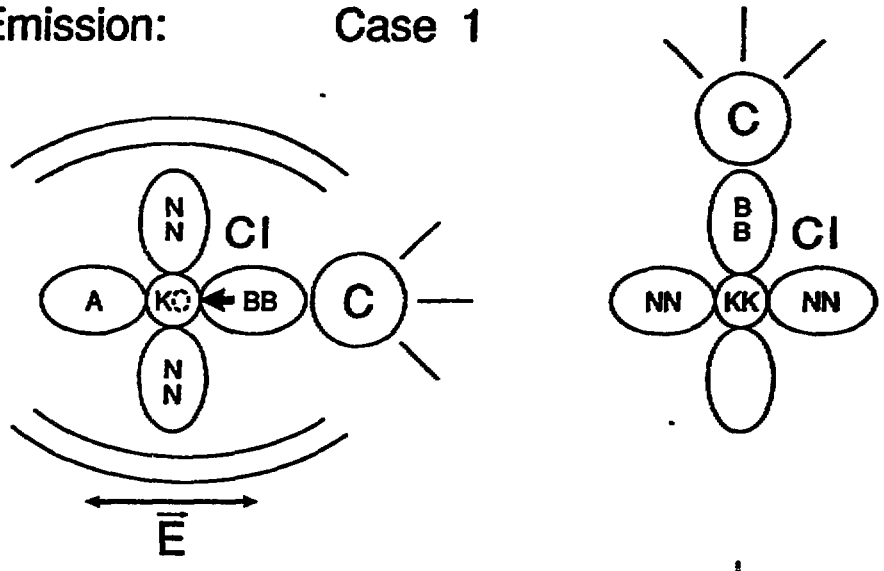

Case 2

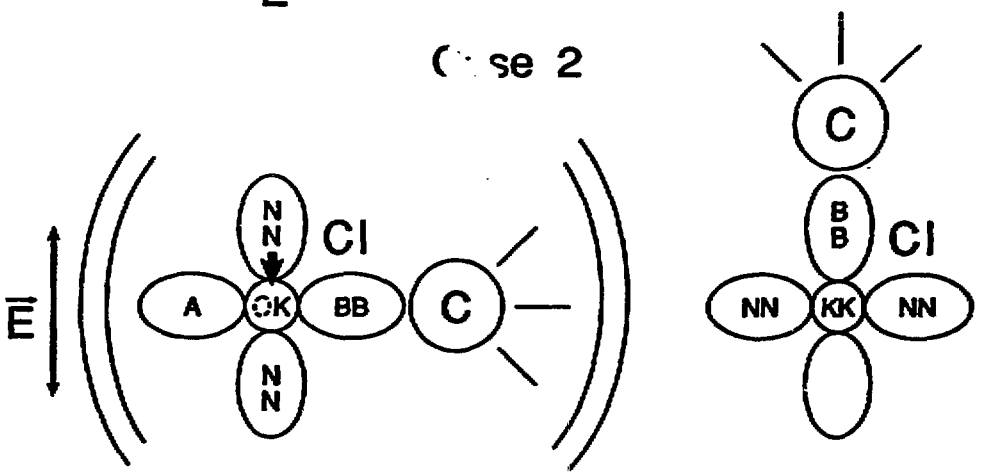

Fig 10

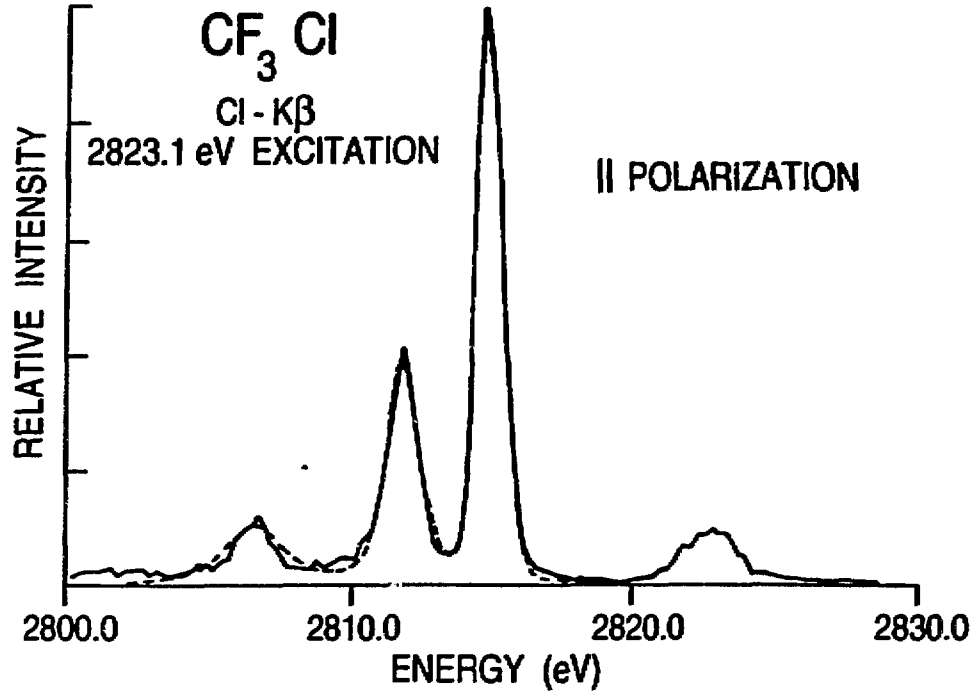
CF_3Cl
Cl - Kβ
2823.1 eV EXCITATION
∥ POLARIZATION
RELATIVE INTENSITY
2800.0
2810.0
2820.0
2830.0
ENERGY (eV)

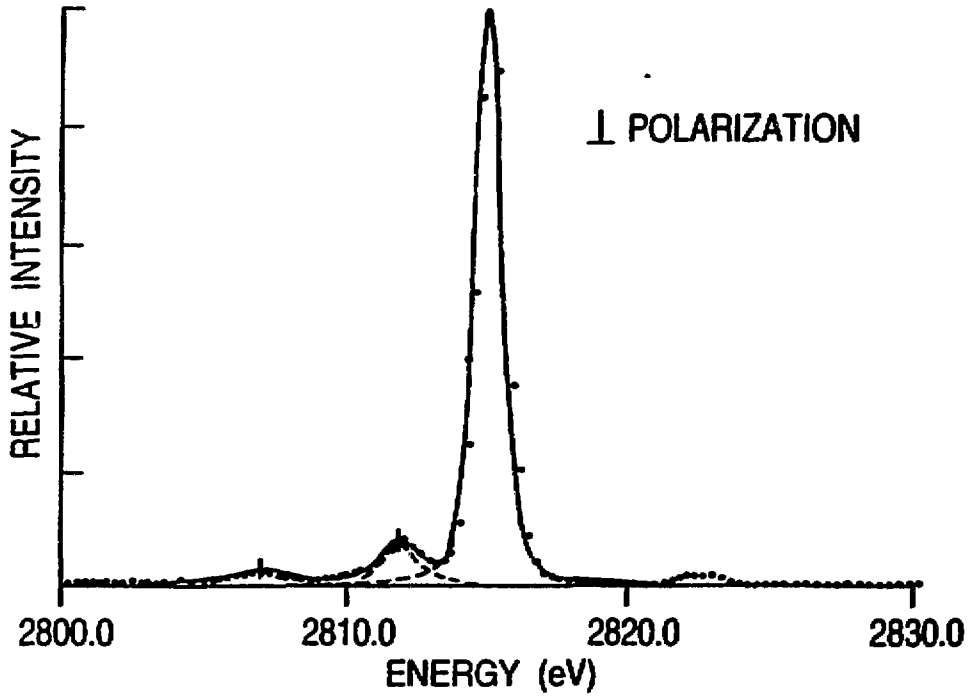
⊥ POLARIZATION
RELATIVE INTENSITY
2800.0
2810.0
2820.0
2830.0
ENERGY (eV)

Fig 11a5

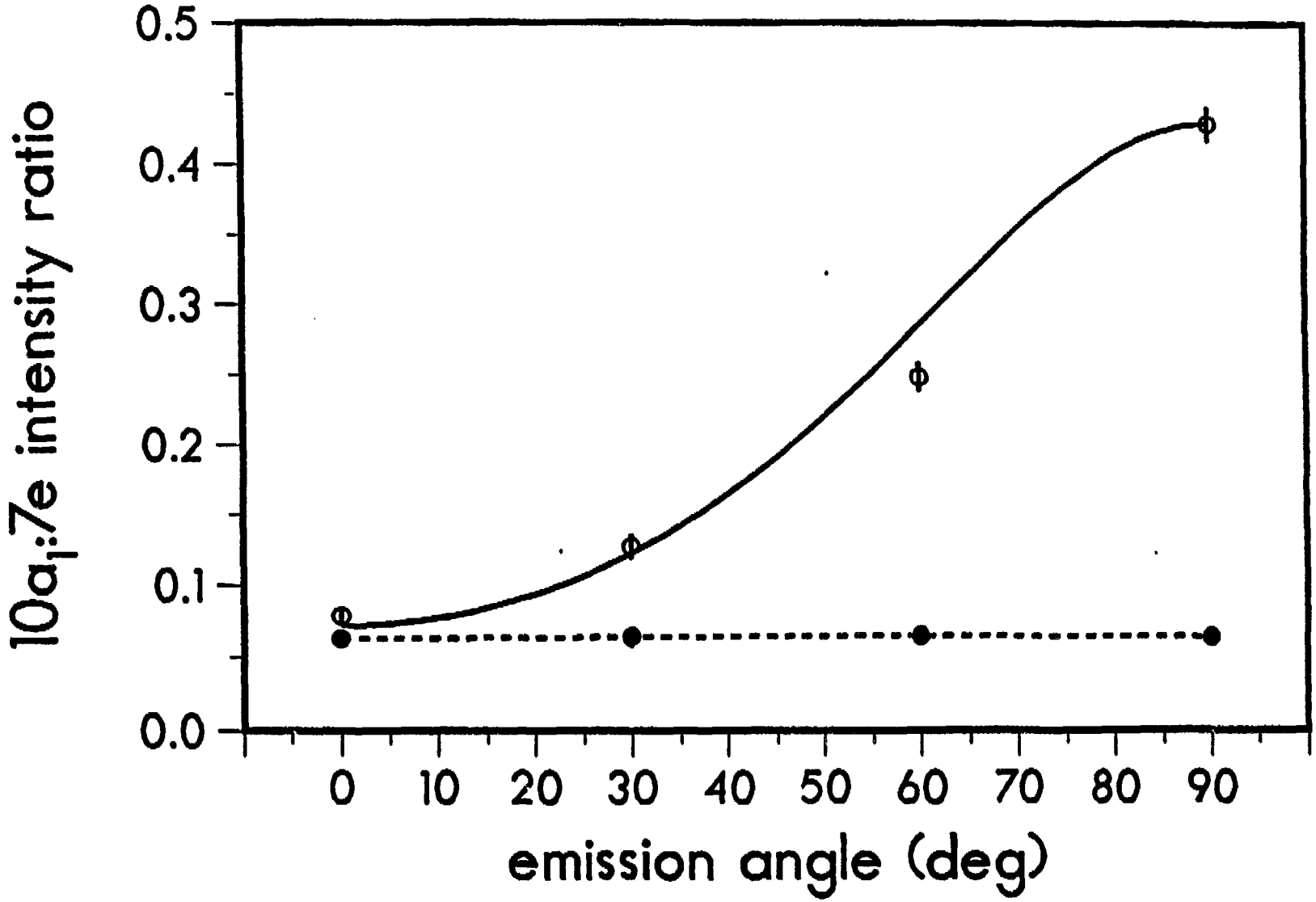
0.5
0.4
0.3
0.2
0.1
0.0
$10a_1:7e$ intensity ratio
0
10
20
30
40
50
60
70
80
90
emission angle (deg)

Fig 12

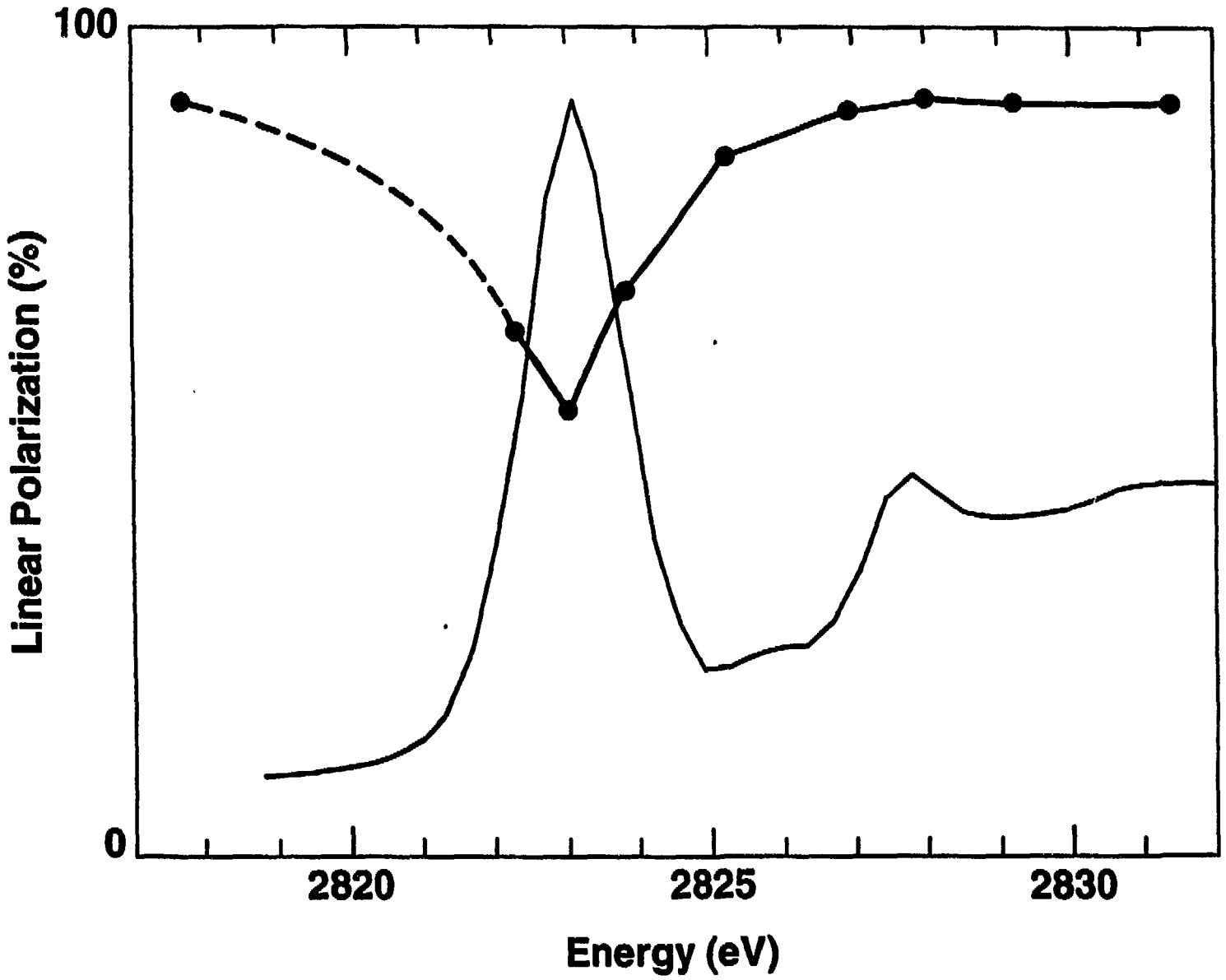
ELASTIC SCATTERING FROM $CFCl_3$
100
0
Linear Polarization (%)
2820
2825
2830
Energy (eV)

Fig 13